Catal Lett (2009) 127:377–385
DOI 10.1007/s10562-008-9693-0

Cobalt and Copper Composite Oxides as Efficient Catalysts for Preferential Oxidation of CO in H_2-Rich Stream

Debing Li · Xianhong Liu · Qinghong Zhang · Ye Wang · Huilin Wan

Received: 24 July 2008 / Accepted: 19 September 2008 / Published online: 11 November 2008

Abstract A series of Co–Cu composite oxides with different Co/Cu atomic ratios were prepared by a co-precipitation method. XRD, N_2 sorption, TEM, XPS, H_2-TPR, CO-TPR, CO-TPD and O_2-TPD were used to characterize the structure and redox properties of the composite oxides. Only spinel structure of Co_3O_4 phase was confirmed for the Co–Cu composite oxides with Co/Cu ratios of 4/1 and 2/1, but the particle sizes of these composite oxides decreased evidently compared with Co_3O_4. These composite oxides could be reduced at lower temperatures than Co_3O_4 by either H_2 or CO. CO and O_2 adsorption amounts over the composite oxides were significantly higher than those over Co_3O_4. These results indicated a strong interaction between cobalt and copper species in the composite samples, possibly suggesting the formation of $Cu_xCo_{3-x}O_4$ solid solution. For the preferential oxidation of CO in a H_2-rich stream, the Co–Cu composite oxides (Co/Cu = 4/1–1/1) showed distinctly higher catalytic activities than both Co_3O_4 and CuO, and the formation of $Cu_xCo_{3-x}O_4$ solid solution was proposed to contribute to the high catalytic activity of the composite catalysts. The Co–Cu composite oxide was found to exhibit higher catalytic activity than several other Co_3O_4-based binary oxides including Co–Ce, Co–Ni, Co–Fe and Co–Zn oxides.

Keywords Co–Cu composite oxide · CO oxidation · Co_3O_4 · Preferential oxidation of CO

D. Li · X. Liu · Q. Zhang (✉) · Y. Wang · H. Wan
State Key Laboratory of Physical Chemistry of Solid Surfaces, Department of Chemistry, College of Chemistry and Chemical Engineering, Xiamen University, Xiamen 361005, China
e-mail: zhangqh@xmu.edu.cn

1 Introduction

Catalytic preferential oxidation (PROX) of CO in a H_2-rich stream has recently attracted much attention, since it is considered as the simplest and the most effective method for CO removing from the gas mixtures containing concentrated H_2 for fuel cells [1–3]. Noble metal catalysts, including Pt, Ru, Rh, Pd and Au, have shown high activities and good stabilities for the PROX of CO [4–9]. However, noble metal catalysts inevitably have disadvantages of high cost and limited availability. Moreover, the selectivity for CO oxidation in H_2-rich gas mixtures over noble metal catalysts may decrease at high reaction temperatures [5, 9]. Therefore, it is highly desirable to develop efficient non-noble transition metal oxide catalysts for the PROX of CO [10–17].

Co_3O_4 has been reported to be one of the most promising non-noble metal oxide catalysts for CO oxidation without H_2 in the reaction gas stream at low temperatures [18–20]. However, studies on Co_3O_4 catalyst for the PROX of CO in H_2-rich stream are scarce [12–14]. Yung et al. [12] studied the PROX of CO over a CoO_x/ZrO_2 catalyst under various reaction conditions and found that the CoO_x/ZrO_2 catalyst showed high CO conversion and high selectivity of CO oxidation in a temperature window of 80–200 °C. Recently, Guo and Liu [13, 14] reported that high CO conversion activity could be achieved over a Co_3O_4–CeO_2 catalyst. They also indicated that the addition of MnO_x could promote the interaction between Co_3O_4 and CeO_2, and thus increase the Co^{3+} content in the catalyst, which may enhance the selectivity for CO oxidation [14]. On the other hand, CuO is also known to be one of the main active components for the PROX of CO, and a few studies have been contributed to CuO–CeO_2 catalysts [15–17]. Luo et al. [16] reported that the CuO–CeO_2

catalyst with a high surface area exhibited a high activity in the PROX of CO and they argued that finely dispersed CuO species were the active sites.

Co_3O_4 generally takes the spinel structure (AB_2O_4) based on a cubic closely-packed structure of oxide ions, in which Co (II) ions occupy the tetrahedral sites and Co (III) ions occupy the octahedral sites [21]. Spinel compounds have shown efficient catalytic performances in various reactions because of the unique cation distributions in tetrahedral and octahedral sites [22–26]. Co–Cu composite oxide with spinel structure ($Cu_xCo_{3-x}O_4$) was proven to be excellent for the oxidative elimination of volatile organic compounds (e.g., hexane) [26].

Therefore, we expect that the Co–Cu composite oxides may function as efficient catalysts for the PROX of CO. However, to the best of our knowledge, there is no systematic study on the PROX of CO over the Co–Cu composite oxides. In this work, we report the catalytic performances of the Co–Cu composite oxides prepared by a co-precipitation method for the PROX of CO. The catalysts will be characterized in detail to gain insight into the structure-performance correlation. The catalytic property of the Co–Cu composite oxide will also be compared with other binary composite oxides such as Co–Ce, Co–Ni, Co–Fe and Co–Zn oxides.

2 Experimental

2.1 Preparation of Co–Cu Composite Oxides

Co–Cu composite oxides with different Co/Cu atomic ratios were prepared by the co-precipitation method [13, 27]. Typically, a mixed aqueous solution of $Co(NO_3)_2$ (0.2 mol/L) and $Cu(NO_3)_2$ (0.2 mol/L) with a fixed Co/Cu ratio was added into an aqueous solution of Na_2CO_3 (0.5 mol/L), and a suspension was obtained. Then, the pH of the suspension was adjusted to $\sim$8.5 by ammonia solution. After further aging for 4 h, the solid was recovered by filtration followed by washing with hot deionized water and then drying at 80 °C for 24 h. The Co–Cu composite oxides were finally obtained by calcination in air at 350 °C for 5 h. Co_3O_4 and CuO single oxides and other Co–M (M = Ce, Zn, Ni, Fe) composite oxides were prepared with the same procedure.

2.2 Characterization of Catalysts

X-ray diffraction (XRD) patterns were collected on a Panalytical X' pert Pro type powder diffractometer using Cu Kα radiation (40 kV, 30 mA). N_2 sorption isotherms were obtained at 77 K on a Micromeritics Tristar 3000 surface and porosimetry analyzer. The surface area, pore volume and pore size distribution were evaluated by the BET [28] and BJH [29] methods from the desorption branch of the isotherm.

TEM observations were performed on a Tecnai F30 electron microscope (Phillips Analytical) operated at an acceleration voltage of 300 kV. Samples for TEM measurements were suspended in ethanol and dispersed ultrasonically. Drops of the suspensions were applied on a copper grid coated with carbon. X-ray photoelectron spectroscopic (XPS) measurements were performed with a Multilab 2000 system (Thermo Electron Co.) using Al-Kα radiation (1846.6 eV) as X-ray source to investigate the oxidation states of Co and Cu in the Co–Cu composite oxides. The surface Co/Cu ratio was estimated from the peak areas and the sensitivity factor presented by Physical Electronics.

The redox properties of Co–Cu composite oxide catalysts were studied by temperature-programmed reduction techniques including H_2-TPR and CO-TPR with a Micromeritics Auto Chem 2920 II instrument. Typically, the sample (15 mg) was placed in a quartz reactor, and was heated from 40 to 850 °C at a rate of 10 °C/min in H_2- or CO-containing He gas flow. The amount of H_2 consumption was measured using a thermal conductivity detector (TCD), and the amount of CO consumption was measured using a Pfeiffer Vacuum ThermoStar mass spectrometer with a signal of $m/e = 28$.

The adsorption properties of Co–Cu composite oxide catalysts were investigated by temperature-programmed desorption techniques including CO-TPD and O_2-TPD. The experiments were performed on the same equipment for TPR measurements. 200 mg of sample was used for a typical analysis. After pretreated at 350 °C in a 20% O_2/He flow for 1 h, the samples were switched to a He flow, and cooled down to 50 °C. CO and O_2 adsorption were carried out by exposing the sample to a flow of 5% CO/He or 10% O_2/He at 50 °C. After removing CO or O_2 in gas phase by He purge, the CO-TPD or O_2-TPD was carried out in He flow by heating up to 600 °C at a rate of 10 °C/min.

2.3 Catalytic Reaction

Catalytic reactions (PROX of CO) were carried out using a fixed-bed reactor (8 mm i.d.) at atmospheric pressure. Before reaction, the catalysts were pretreated in an O_2 containing He gas flow at 200 °C for 40 min. The feed gas was comprised of 1% CO, 1% O_2, and 50% H_2 (vol.%) balanced with He. The space velocity was 30,000 mL/g/h (corresponding to 100 mg catalyst and 50 cm^3/min). The inlet and outlet gas compositions were analyzed by an on-line gas chromatograph equipped with TCD and FID. H_2, O_2, CO and CO_2 were separated using a carbon molecular sieve (TDX-01) column. CO and CO_2 were further converted to methane by a methanation reactor and

analyzed using a FID detector. The carbon balance in each run was 100 ± 3%.

The conversion of CO to CO_2 and the selectivity of O_2 for CO oxidation (forming CO_2) in H_2-rich stream were calculated as follows:

$$\text{CO conversion}\,(\%) = \frac{[\text{CO}]_{\text{in}} - [\text{CO}]_{\text{out}}}{[\text{CO}]_{\text{in}}} \times 100\%$$

$$\text{Selectivity}\,(\%) = \frac{1/2[\text{CO}_2]}{[\text{O}_2]_{\text{in}} - [\text{O}_2]_{\text{out}}} \times 100\% = \frac{1/2([\text{CO}]_{\text{in}} - [\text{CO}]_{\text{out}})}{[\text{O}_2]_{\text{in}} - [\text{O}_2]_{\text{out}}} \times 100\%$$

3 Results and Discussion

3.1 Structure of Co–Cu Composite Oxides

Figure 1 shows the XRD patterns of the Co–Cu composite oxides with different Co/Cu ratios along with Co_3O_4 and CuO. All the diffraction peaks of Co_3O_4 can be ascribed to the cubic spinel structure of Co_3O_4 [24], while those of CuO are assignable to the monoclinic tenorite structure [30]. For the Co–Cu composite oxides with Co/Cu ratios of 4/1 and 2/1, only diffraction peaks ascribed to the spinel phase of Co_3O_4 could be observed, but these diffraction peaks became significantly weaker and broader as compared with those of Co_3O_4. The broadening of the diffraction peaks indicates that the crystallite sizes of composite oxides become smaller. We have estimated the crystallite sizes of these two samples by the Scherrer equation. The result summarized in Table 1 clearly shows that the crystallite sizes of the composite oxides with Co/Cu ratios of 4/1 and 2/1 are significantly smaller than that of Co_3O_4 alone. With a further decrease in the Co/Cu ratio to 1/1, the diffraction peaks attributed to Co_3O_4 and CuO were both observed, and as the Co/Cu ratio decreased to 1/4, only monoclinic tenorite structure of CuO phase could be observed.

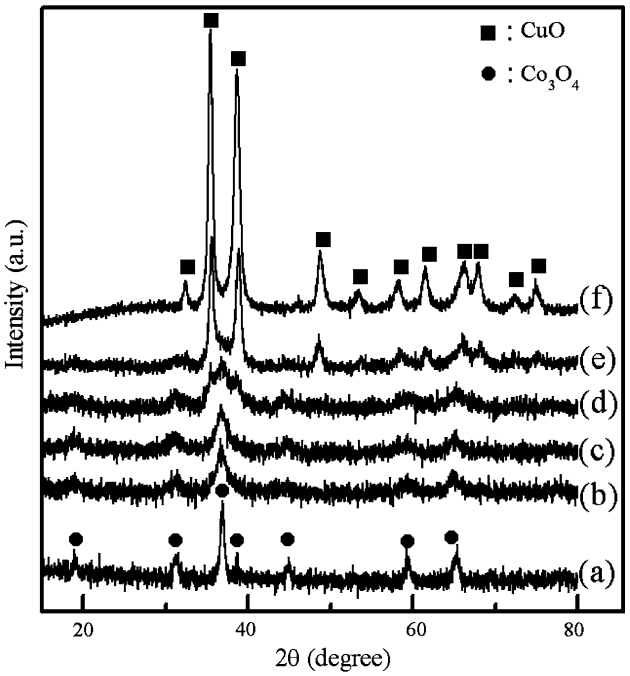

Fig. 1 XRD patterns of Co–Cu composite oxides with different Co/Cu ratios. (a) Co_3O_4; (b) Co–Cu–O (Co/Cu = 4/1); (c) Co–Cu–O (Co/Cu = 2/1); (d) Co–Cu–O (Co/Cu = 1/1); (e) Co–Cu–O (Co/Cu = 1/4); (f) CuO

As mentioned before, in the spinel structure of Co_3O_4, Co^{3+} occupies the octahedral site and Co^{2+} occupies the tetrahedral site in cubic closely-packed structure of O^{2-}, where the ratio of Co^{3+}/Co^{2+} is 2/1. As Cu^{2+} possesses the same ionic charge and similar ionic diameter ($D_{Cu^{2+}} = 73$ pm) to Co^{2+} ($D_{Co^{2+}} = 74.5$ pm), we speculate that Cu^{2+} could replace Co^{2+} entering the cubic structure of Co_3O_4 (maybe forming $Cu_xCo_{3-x}O_4$ solid solution with the spinel structure). The maximum number of Cu^{2+} accommodated by $Cu_xCo_{3-x}O_4$ with spinel structure was at Co/Cu ratio of 2/1, where Co^{2+} in Co_3O_4 was totally replaced by Cu^{2+}. Actually, from the XRD patterns of Co–Cu–O composites with Co/Cu ratios of 4/1 and 2/1, only the diffraction peaks attributed to the spinel structure were observed, and no peaks of CuO could be discerned. Thus, we speculate that $Cu_xCo_{3-x}O_4$ solid solution with spinel structure was possibly formed in these two samples [26, 31].

Figure 2 shows N_2 sorption isotherms and the pore size distributions for the Co–Cu composite oxides along with Co_3O_4 and CuO. The calculated BET surface area and mean pore size of these samples are also listed in Table 1. All of the samples exhibited the type IV isotherms, which indicated the existence of mesopores probably due to the aggregation of nano particles. From Table 1 and Fig. 2, it can be seen that the BET surface areas increase from 52 m^2/g for Co_3O_4 to 100 m^2/g for the Co–Cu composite oxide with Co/Cu ratio of 2/1, while the pore size decreases from 13 to 9.6 nm simultaneously. These changes likely arise from the decrease in the particle size of the composite oxide. With a further increase in Cu content, the crystalline CuO was formed, and the BET surface area declined. CuO possesses the lowest BET surface area.

Figure 3 shows the TEM images of Co_3O_4, the Co–Cu composite oxides with Co/Cu ratios of 4/1 and 2/1, and CuO and the particle size distributions derived by counting ca. 100 particles for each sample. The TEM images clearly show that all these samples are nanoparticles in morphology. It is clear that the mean particle sizes of the Co-Cu composite oxides are significantly smaller than those of Co_3O_4 and CuO. This observation is consistent with the XRD results in essence (Table 1).

Table 1 Physical properties of Co–M composite oxides samples

Sample[a]	Crystallite size[b] (nm)	Mean particle size[c] (nm)	S_{BET}[d] (m^2/g)	Pore size[d] (nm)
Co_3O_4	19	19.5	52	13
Co–Cu–O (4/1)	5	9.0	92	11
Co–Cu–O (2/1)	6	8.5	100	9.6
Co–Cu–O (1/1)	–	–	68	12
Co–Cu–O (1/4)	13	–	43	19
CuO	20	25.5	20	26
Co–Fe–O (4/1)	10	–	97	9
Co–Zn–O (4/1)	6	–	122	7
Co–Ni–O (4/1)	9	–	100	9
Co–Ce–O (4/1)	7	–	110	10

[a] The number in the parenthesis is the atomic ratio of Co/M, where M means Co, Fe, Zn, Ni or Ce

[b] Calculated by the Scherrer equation with the (311) diffraction ($2\theta = 36.9°$) of spinel structure for Co_3O_4, and the Co–Cu composite oxides with Co/Cu ratios of 4/1 and 2/1, and with the (002) diffraction ($2\theta = 35.4°$) of monoclinic tenorite structure for CuO, and the Co–Cu composite oxide with a Co/Cu ratio of 1/4

[c] Calculated from the TEM micrographs by counting ca. 100 particles

[d] Calculated from the desorption branch of the N_2 sorption isotherms

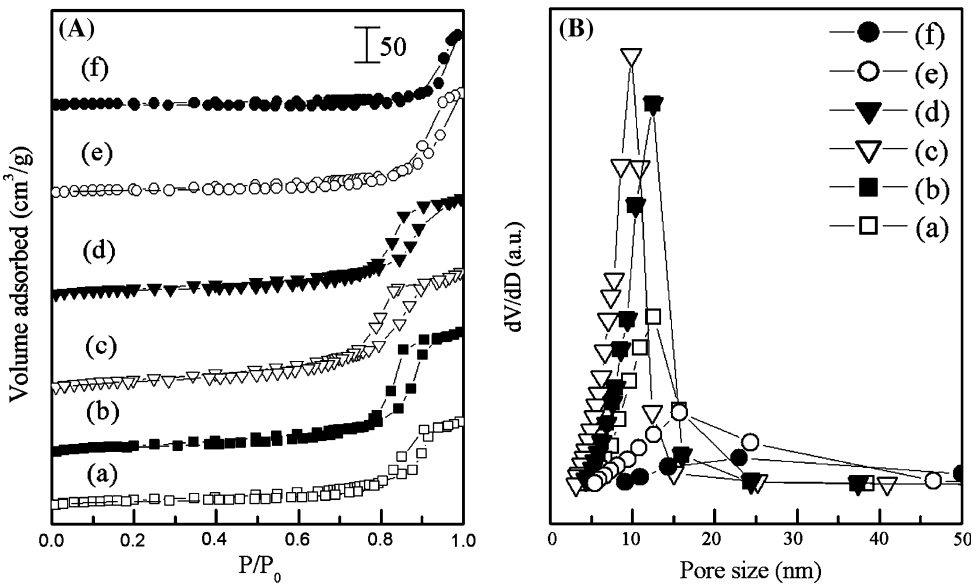

Fig. 2 N_2 adsorption–desorption isotherms (**A**) and pore size distribution (**B**) for Co–Cu composite oxides with different Co/Cu ratios. (a) Co_3O_4; (b) Co–Cu–O (Co/Cu = 4/1); (c) Co–Cu–O (Co/Cu = 2/1); (d) Co–Cu–O (Co/Cu = 1/1); (e) Co–Cu–O (Co/Cu = 1/4); (f) CuO

XPS measurements were performed to investigate the oxidation states of Co and Cu in the Co–Cu composite oxides. The Co $2p_{3/2}$, Cu $2p_{3/2}$ and O 1 s spectra are displayed in Fig. 4 and the binding energy (BE) values along with the surface Co/Cu ratios for the composite oxides calculated from XPS are summarized in Table 2. The BE values of Co $2p_{3/2}$ for all the composite oxides were 779.8–780.2 eV, which were close to that for Co_3O_4 (779.6 eV) [32]. The BE values of Cu $2p_{3/2}$ for all these composite oxides were 932.8–933.0 eV, which were similar to that for CuO (933.1 eV). Therefore, the oxidation states of Co and Cu in the Co–Cu composite oxides were not significantly different from those in single Co_3O_4 and CuO. The O1 s spectra for all the samples in Fig. 4C showed an intense peak at 529.3–529.9 eV and a shoulder at 531.1–531.4 eV. However, the BE values of the intense peak of O1 s for the composite oxides (~529.3 eV) were lower than that for the single Co_3O_4 (529.9 eV) and CuO (529.8 eV). This decrease in the BE may arise from the existence of high-concentration cation vacancy in the Co–Cu composite oxides. Moreover, for the composite oxides, the relative intensity of the shoulder O1 s component (531.4 eV) was higher, and this shoulder is regarded to be associated with the sites possessing lower coordination number of oxygen

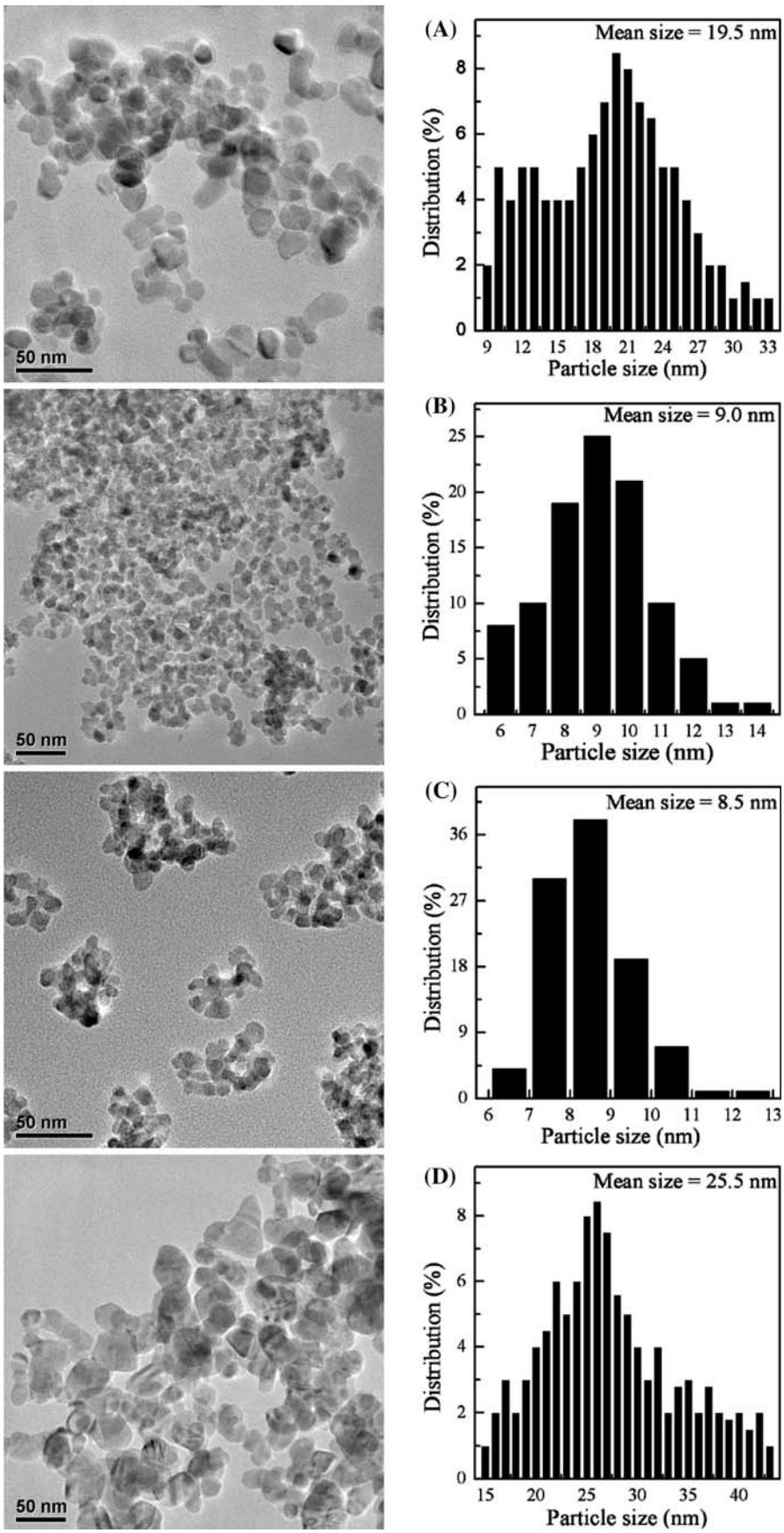

Fig. 3 TEM images of Co_3O_4 (**A**), the Co–Cu composite oxides with Co/Cu ratios of 4/1 (**B**) and 2/1 (**C**), and CuO (**D**)

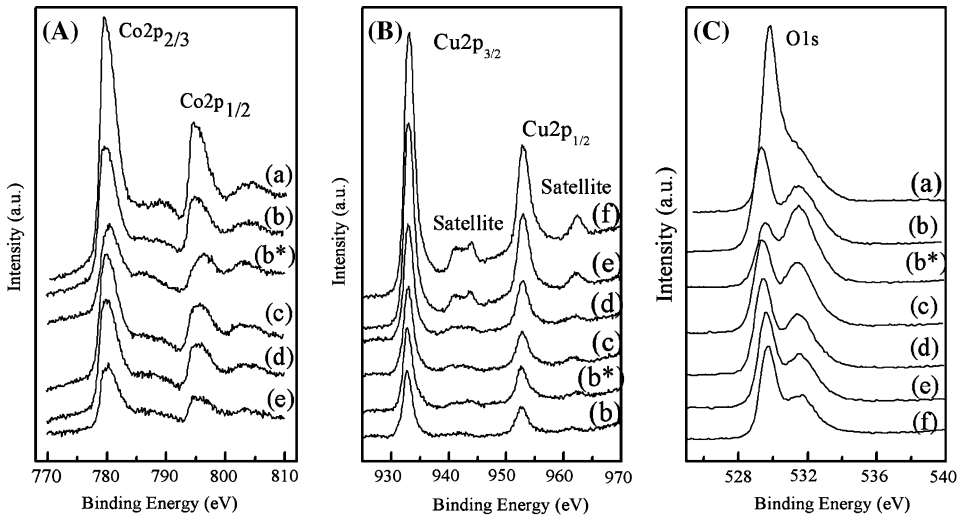

Fig. 4 XPS spectra of Co 2p (**A**), Cu 2p (**B**) and O1 s (**C**) for Co_3O_4 (a), the Co–Cu–O composites with Co/Cu ratios of 4/1 (b), 2/1 (c), 1/1 (d), 1/4 (e), CuO (f), and the used Co–Cu–O (Co/Cu = 4/1) catalyst (b*)

Table 2 XPS results for the Co–Cu composite oxides along with Co_3O_4 and CuO

Sample	Binding energy (eV)			Co/Cu atomic ratio	
(Co/Cu)	O 1s	Co $2p_{3/2}$	Cu $2p_{3/2}$	Bulk	XPS
Co_3O_4	529.9 (67%)[a]	779.6	–	–	–
	531.1 (33%)[a]				
Co–Cu–O (4/1)	529.3 (57%)[a]	779.8	933.0	4	4.4
	531.5 (43%)[a]				
Co–Cu–O (2/1)	529.4 (56%)[a]	780.0	932.9	2	2.9
	531.4 (44%)[a]				
Co–Cu–O (1/1)	529.6 (59%)[a]	780.0	932.9	1	1.9
	531.4 (41%)[a]				
Co–Cu–O (1/4)	529.7 (61%)[a]	780.2	932.8	0.25	0.5
	531.4 (39%)[a]				
CuO	529.8 (67%)[a]	–	933.1	–	–
	531.3 (33%)[a]				

[a] Relative percentage in the parenthesis

ions [32]. This further suggests the strong interaction between Co_3O_4 and CuO, and the possible formation of $Cu_xCo_{3-x}O_4$ solid solution. From Table 2, it can be seen that the surface Co/Cu ratios of the composite oxides were slightly higher than its corresponding bulk values, suggesting the enrichment of Co on the surface of the composite oxides.

Figure 5A shows the H_2-TPR profiles of the samples. Co_3O_4 alone exhibited a well-defined two-step reduction, and the reduction peaks were observed at 285 and 350 °C. These two H_2 consumption peaks could be ascribed to the two-step reduction of Co_3O_4 to metallic Co, i.e., $Co^{3+} \rightarrow Co^{2+}$ and $Co^{2+} \rightarrow Co^0$ [33]. CuO was reduced at lower temperatures than Co_3O_4, and the main reduction peak was located at 250 °C. The reduction of the Co–Cu composite oxides occurred at temperatures significantly lower than those for Co_3O_4 and quite similar to those for CuO. For example, the main reduction peak for the Co–Cu composite oxide with a Co/Cu ratio of 4/1 was observed at 245 °C, which was ~100 °C lower than that for Co_3O_4 (350 °C). In other words, the presence of a small amount of copper in the composite oxide could remarkably promote the reduction of Co_3O_4. We speculate that this further supports the formation of $Cu_xCo_{3-x}O_4$ solid solution in the composite [33]. This speculation has further been confirmed by comparing the H_2-TPR profile of the Co-Cu composite oxide prepared by the co-precipitation with that of the mechanical mixture of Co_3O_4 and CuO with the same Co/Cu ratio (4/1) (Fig. 5A, g). Three separated H_2 consumption peaks were observed for the mechanical mixture, while the composite oxide gave only one H_2 consumption.

Figure 5B shows the CO-TPR profiles of the Co–Cu composite oxide (Co/Cu = 4/1), Co_3O_4 and CuO. Similar to the H_2-TPR results, the reduction of CuO by CO proceeded at lower temperatures than that of Co_3O_4. The Co–Cu composite oxide could also be reduced at lower temperatures than Co_3O_4. This can also be explained by assuming the formation of $Cu_xCo_{3-x}O_4$ solid solution in the composite oxide.

CO-TPD (Fig. 6A) and O_2-TPD (Fig. 6B) were performed to study the adsorptions of CO and O_2 on the Co–Cu composite oxides. Almost no CO was adsorbed on CuO. On the other hand, a significant portion of CO was desorbed as CO_2 from both the Co–Cu composite oxide (Co/Cu = 4/1) and Co_3O_4, the ratio of CO_2/CO desorbed from Co_3O_4 was 20 while that from the Co–Cu composite oxide (Co/Cu = 4/1) was 5.0. However, compared with Co_3O_4, a remarkably larger amount of CO was found adsorbed on the Co-Cu composite oxide. The total

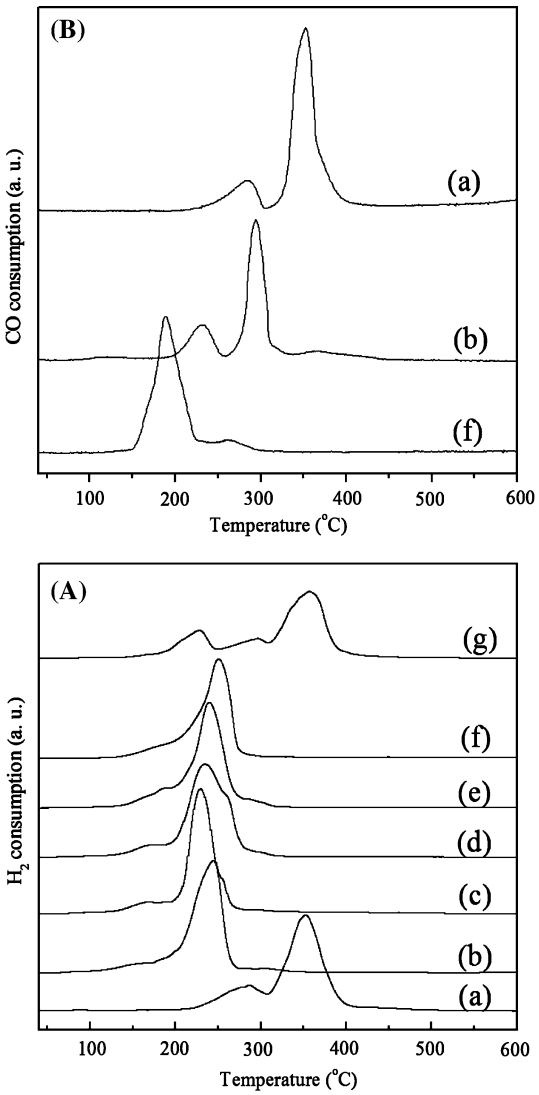

Fig. 5 H_2-TPR (**A**) and CO-TPR (**B**) profiles of Co–Cu composite oxides with different Co/Cu ratios along with Co_3O_4 and CuO. (a) Co_3O_4; (b) Co–Cu–O (Co/Cu = 4/1); (c) Co–Cu–O (Co/Cu = 2/1); (d) Co–Cu–O (Co/Cu = 1/1); (e) Co–Cu–O (Co/Cu = 1/4); (f) CuO; (g) mechanical mixture of Co_3O_4 and CuO with the Co/Cu ratio of 4/1

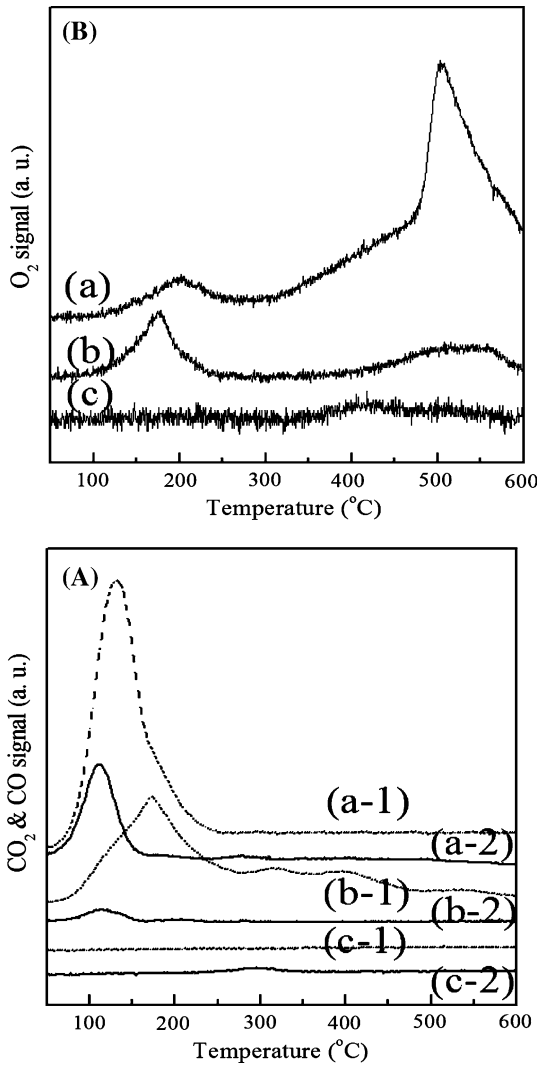

Fig. 6 CO-TPD (**A**) and O_2-TPD (**B**) profiles over the Co–Cu composite oxide with the Co/Cu = 4/1 (a), Co_3O_4 (b) and CuO (c). In profile (**A**), CO_2 (*broken line*) and CO (*solid line*) were desorbed after CO adsorption

desorption amount including CO and CO_2 from the Co–Cu composite oxide (Co/Cu = 4/1) was 1.7 times per surface area (3 times per gram) of that from Co_3O_4. The higher CO adsorption capacity of the Co–Cu composite oxide may enhance its catalytic performance in the PROX of CO. The O_2 adsorption amount on the Co–Cu composite oxide was also higher than that on Co_3O_4, whereas CuO could not adsorb O_2 (Fig. 6B).

3.2 Catalytic Performance of Co–Cu Composite Oxides for the PROX of CO

Figure 7 shows the catalytic performances of the Co–Cu composite oxide catalysts with different Co/Cu ratios for PROX of CO in a H_2-rich stream. Co_3O_4 single oxide exhibited a better catalytic activity than CuO. CO in the gas mixture could not be completely oxidized over both Co_3O_4 and CuO catalyst at any reaction temperature. The Co–Cu composite oxides with Co/Cu ratios of 4/1, 2/1, and 1/1 showed higher CO conversions than Co_3O_4 and CuO at $\leq$150 °C. Particularly, the catalyst with a low Cu content (Co/Cu = 4/1) could accelerate the conversion of CO very efficiently; at 125 °C, CO conversion reached 100% over this composite oxide, and the selectivity toward CO oxidation was ~70%. When the temperature was increased to >150 °C, CO conversion over these three catalysts dropped. We found that, under such conditions, the oxidation of hydrogen turned into the main reaction and the O_2 selectivity for CO oxidation decreased sharply. The composite oxide with a Co/Cu ratio of 1/4 exhibited lower CO

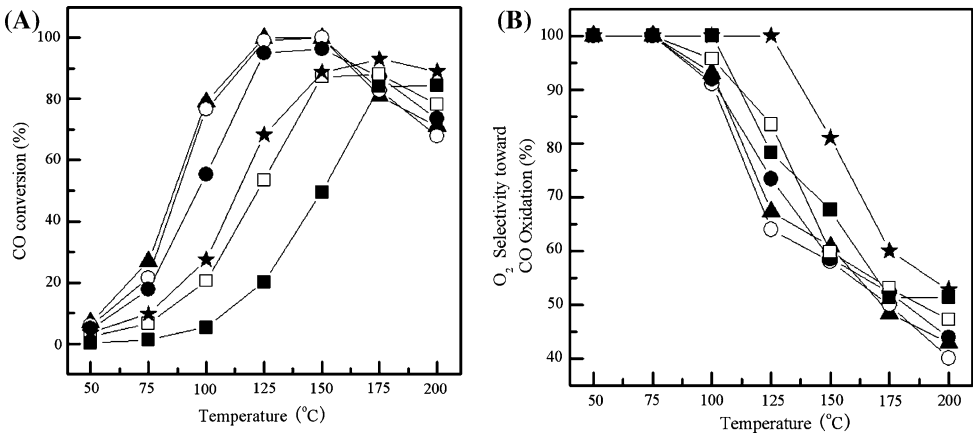

Fig. 7 Preferential oxidation of CO in a H_2-rich stream over Co–Cu catalysts with different Co/Cu ratios: CO conversion (**A**) and O_2 selectivity toward CO oxidation (**B**) (★: Co_3O_4, ▲: Co–Cu–O (Co/Cu = 4/1), ○: Co–Cu–O (Co/Cu = 2/1), ●: Co–Cu–O (Co/Cu = 1/1), □: Co–Cu–O (Co/Cu = 1/4), ■: CuO)

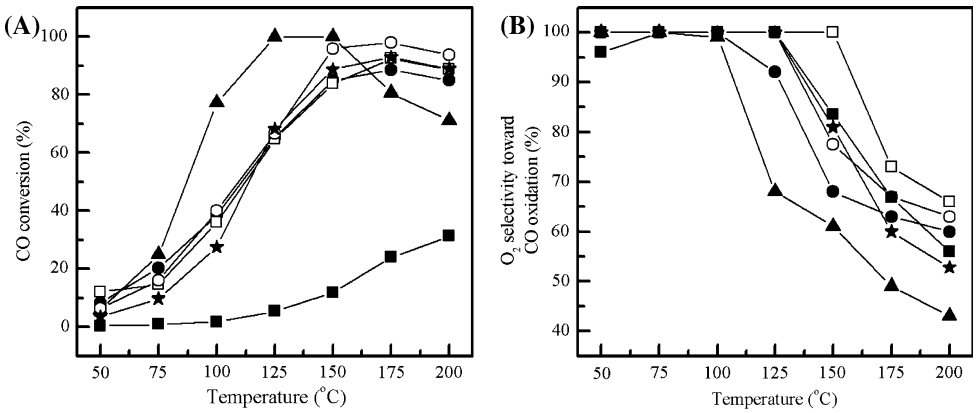

Fig. 8 Catalytic performances of the Co–M binary oxide catalysts (Co/M = 4/1) and Co_3O_4 for the PROX of CO. CO conversion (**A**) and O_2 selectivity toward CO oxidation (**B**) (▲: the Co–Cu composite oxide, ○: the Co–Ce composite oxide, ●: the Co–Zn composite oxide, □: the Co–Ni composite oxide, ■: the Co–Fe composite oxide, ★: Co_3O_4)

conversions than Co_3O_4 at most reaction temperatures. Among all the tested catalysts, Co_3O_4 was superior in the selectivity of O_2 for CO conversion. We have confirmed that the CO conversion and O_2 selectivity to CO oxidation kept stable during 32 h reaction test at 125 °C over Co–Cu–O (Co/Cu = 4/1) catalyst. The XPS spectra of this used catalyst (Fig. 4b*) showed that oxidation states of Co and Cu species were not significantly different from that in the catalyst before the reaction.

We have also examined the catalytic performances of Co_3O_4-based other composite oxides including Co–Fe, Co–Zn, Co–Ni and Co–Ce oxides with a Co/M ratio of 4/1 for the PROX of CO, and structure properties of these samples including surface area were listed in Table 1. As shown in Fig. 8, the Co–Fe composite oxide showed very low CO conversion, and the composite oxides of Co–Zn and Co–Ni only exhibited similar performances as Co_3O_4. Co–Ce composite oxide could provide higher CO conversions than Co_3O_4, but it was less active than the Co–Cu composite oxide.

The results described above demonstrate that the Co–Cu composite oxide with a proper Co/Cu ratio is quite unique for the PROX of CO. Over the Co–Cu composite oxide with a Co/Cu ratio of 4/1, CO conversion was almost 100% at 125 °C, which was significantly higher than those over Co_3O_4 and CuO alone, and was also higher than other Co_3O_4-based binary oxides. To the best of our knowledge, this is the first report to show the high activity of Co–Cu composite oxides in the PROX of CO. We speculate that the formation of $Cu_xCo_{3-x}O_4$ solid solution in the composite oxide, as suggested by XRD, TEM, H_2-TPR and CO-TPR characterizations, may contribute to the increase in CO conversions.

4 Conclusions

The Co–Cu composite oxide catalysts with proper Co/Cu ratios (4/1–1/1) prepared by a co-precipitation method exhibited significantly better catalytic performances than Co_3O_4 and CuO alone for the preferential oxidation of CO in a H_2-rich stream. The composite oxide with a Co/Cu ratio of 4/1 could provide 100% CO conversions at 125 °C. Characterizations using XRD, TEM, H_2-TPR and CO-TPR revealed the formation of $Cu_xCo_{3-x}O_4$ solid solution in the composite oxide with Co/Cu ratios of 4/1 and 2/1. The mean particle size of the composite oxides became remarkable smaller than that of Co_3O_4, and the reducibility

was also significantly promoted. The adsorption of CO and O_2 was remarkably enhanced over the composite oxide. These were proposed to account for the increased CO conversions over the Co–Cu composite oxides. The Co–Cu composite oxide was found to exhibit higher catalytic activity than other Co_3O_4-based binary oxides such as Co–Ce, Co–Ni, Co–Fe and Co–Zn oxides.

Acknowledgments This work was supported by the National Natural Science Foundation of China (20773099), the National Basic Research Program of China (2005CB221408), the Key Scientific Project of Fujian Province of China (No. 2005HZ01-3), and the Program for New Century Excellent Talents in Fujian province (to Q. Zhang).

References

1. Steele BCH, Heinzel A (2001) Nature 414:345
2. Ratnasamy P, Srinivas D, Satyanarayana CVV, Manikandam P, Kumaran R, Senthil S, Sachin M, Shetti VN (2004) J Catal 221:455
3. Choudhary TV, Goodman DW (2002) Catal Today 77:65
4. Sanchez RMT, Ueda A, Tanaka K, Haruta M (1997) J Catal 168:125
5. Kahlich MJ, Gasteiger HA, Behm RJ (1997) J Catal 171:93
6. Son IH, Shamsuzzoha M (2002) J Catal 210:460
7. Pozdnyakova O, Tesehner D, Wootseh A, Kröhnert J, Steinhauer B, Sauer H, Toth L, Jentoft FC, KnoP-Gericke A, Paäl Z, Schlögl R (2006) J Catal 237:17
8. Tanaka K, Shou M, He H, Shi X (2006) Catal Lett 110:185
9. Iwasa N, Arai S, Arai M (2008) Appl Catal B 79:132
10. Teng Y, Sakurai H, Ueda A, Kobayashi T (1999) Int J Hydrogen Energy 24:355
11. Huang Y, Wang A, Li L, Wang X, Su D, Zhang T (2008) J Catal 255:144
12. Yung MM, Zhao ZK, Woods MP, Ozkan US (2008) J Mol Catal A 279:1
13. GuO Q, Liu Y (2007) React Kinet Catal Lett 92:19
14. GuO Q, Liu Y (2008) Appl Catal B 82:19
15. Moreno M, Baronetti GT, Laborde MA, Mariño FJ (2008) Int J Hydrogen Energy. doi:10.1016/j.ijhydene.2008.03.043
16. Luo MF, Ma JM, Lu JQ, Song YP, Wang YJ (2007) J Catal 246:52
17. Moretti E, Storaro L, Talon A, Patrono P, Pinzari F, Montanari T, Ramis G, Lenarda M (2008) Appl Catal A 344:165
18. Wang YZ, Zhao YX, Gao CG, Liu DS (2007) Catal Lett 116:136
19. Pollard MJ, Weinstock BA, Bitterwolf TE, Griffiths PR, Newbery AP, Paine III JB (2008) J Catal 254:218
20. Wang CB, Tang CW, Gau SJ, Chien SH (2005) Catal Lett 101:59
21. Mocuta C, Barbier A, Renaud G (2000) Appl Surf Sci 56:162
22. Mathew T, Shiju NR, Sreekumar K, Rao BS, Gopinath CS (2002) J Catal 210:405
23. Sreekumar K, Mathew T, Devassy BM, Rajagopal R, Vetrivel R, Rao BS (2001) Appl Catal 205:11
24. Sreekumar K, Mathew T, Rajagopal R, Vetrivel R, Rao BS (2000) Catal Lett 65:99
25. Said AA, Ai-Qasmi R (1996) Thermochim Acta 275:83
26. Zavyalova U, Nigrovski B, Pollok K, Langenhorst F, Müler B, Scholz P, Ondruschka B (2008) Appl Catal B 83:221
27. Porta P, Dragone R, Fierro G, Inversi M, Lo Jacono M, Moretti G (1991) J Mater Chem 1:311
28. Brunauer B, Emmett PH, Teller PHE (1938) J Am Chem Soc 60:309
29. Barrett EP, Joyner LS, Haienda PP (1951) J Am Chem Soc 73:373
30. Zarate RA, Hevia F, Fuentes S, Fuenzalida VM, Zúñiga A (2007) J Solid State Chem 180:1464
31. Cesar DV, Peréz CA, Schmal M, Salim VMM (2000) Appl Surf Sci 157:159
32. Dupin J-C, Gonbeau D, Vinatier P, Levasseur A (2000) Phys Chem Chem Phys 1319
33. Fierro G, Jacono ML, Inversi M, Dragone R, Porta P (2000) Top Catal 10:39